Наносистеми, наноматеріали, нанотехнології
Nanosistemi, Nanomateriali, Nanotehnologii
2026, т. 24, № 1, сс. 123–139
https://doi.org/10.15407/nnn.24.01.0123

PACS numbers: 64.75.Ef, 64.75.Jk, 64.75.Nx, 81.30.Dz, 81.30.Mh, 82.33.Pt, 82.60.Lf

Prediction of the Thermodynamic Stability and Limits of Isomorphous Substitutions in Solid Solutions $Y_{1-x}Ln_xPO_4$, Where Ln = Gd–Lu, Sc

E. I. Get'man[1], O. Yu. Mariichak[1], L. I. Ardanova[2], and S. V. Radio[1]

[1]*Vasyl' Stus Donetsk National University,*
21, 600-Richchia Str.,
UA-21021 Vinnytsia, Ukraine
[2]*Minnesota State University,*
228, Wiecking Center,
56001 Mankato, Minnesota, USA

Using V. S. Urusov's crystal-energy theory of isomorphous miscibility, the mixing energies (interaction parameters), critical decomposition (stability) temperatures, and limits of isomorphous substitutions are calculated, as well as the thermodynamic stability regions of zircon-type orthophosphate solid solutions with the composition $Y_{1-x}Ln_xPO_4$, where Ln—lanthanides or Sc. The contributions to the mixing energy arising from differences in the sizes of the substitutional structural units and from differences in the nature of the chemical bonding of the system components are characterized. A thermodynamic-stability diagram of solid solutions and the corresponding decomposition domes are presented, enabling graphical prediction of the decomposition temperatures of solid solutions for given substitution limits, or the equilibrium substitution limits for a given temperature and thermodynamic-stability region. The results do not contradict the experimental data reported in the literature. They may be helpful in the search for compositions of mixed matrices and activators for new luminescent, laser, and other materials based on $Y_{1-x}Ln_xPO_4$ (Ln = Gd–Lu, Sc) solid solutions, including nanomaterials.

З використанням кристалоенергетичної теорії ізоморфної змішуваности В. С. Урусова розраховано енергії змішання (параметри взаємодії), критичні температури розпаду (стабільности), границі ізоморфних заміщень, а також визначено області термодинамічної стабільности твердих розчинів ортофосфатів зі структурою циркону складу $Y_{1-x}Ln_xPO_4$, де Ln — лантаноїди або Sc. Охарактеризовано внески в енергію змішання, зумовлені відмінностями у розмірах заміщуваних структурних одиниць, а також у характері хемічного зв'язку компонентів систем.

Подано діяграму термодинамічної стабільности твердих розчинів і куполи їхнього розпаду, що дає змогу графічно прогнозувати температури розпаду твердих розчинів за заданими границями заміщення або рівноважні границі заміщення за заданої температури та області термодинамічної стабільности. Результати роботи не суперечать експериментальним літературним даним і можуть бути корисними під час пошуку складів змішаних матриць та активаторів нових люмінесцентних, лазерних та інших матеріялів на основі твердих розчинів $Y_{1-x}Ln_xPO_4$ (Ln = Gd–Lu, Sc), у тому числі й наноматеріялів.

Key words: solid solutions, lanthanides, yttrium, scandium, orthophosphates, isomorphous substitutions, mixing energy, thermodynamic stability, substitution limits.

Ключові слова: тверді розчини, лантаноїди, Ітрій, Скандій, ортофосфати, ізоморфні заміщення, енергія змішання, термодинамічна стабільність, границі заміщень.

(Received 11 August, 2025; in revised form, 18 August, 2025)

1. INTRODUCTION

Solid solutions based on rare-earth element (REE) orthophosphates are promising materials with excellent luminescent properties and high thermal and radiation stability. They are used as scintillation detectors, phosphors for radiography and plasma panels, materials for radioactive waste storage [1], laser media, protective coatings, cements, high-temperature ion exchangers [2], light-emitting diodes, solar panels, thermal barrier coatings, and in optical thermometry [3].

In addition, in recent years, REE orthophosphate-based nanomaterials have begun to find medical applications. Nanocrystals of yttrium orthophosphate (YPO_4) doped with Dy^{3+} ions at various concentrations are considered promising for use in laser-induced hyperthermia of cancerous tumours. The local temperature of nanoparticle powders increases linearly with increasing laser power and Dy^{3+} concentration, enabling high heating and cooling rates. This allows for precise control of the exposure time and minimal doses of laser irradiation on patients [4].

UV phosphors emitting in the 200–280 nm range are of particular interest for medical applications due to their pronounced bactericidal properties, resulting from the coincidence of their emission wavelengths with the range of maximum DNA sensitivity of microorganisms to UV irradiation. Moreover, ultraviolet radiation effectively destroys surface cancer cells without damaging deeper tissues [5]. REE orthophosphates are also employed in drug delivery sys-

tems and as fluorescent labels for visualizing biomolecules and cellular structures [6].

Initially, materials based on individual orthophosphates were used. Later, it was found that 'double' orthophosphates containing two or more rare-earth elements (REEs) in the host lattice are more effective. For example, very high intensity under ultraviolet excitation was observed for the solid solution $Gd_{0.5}Y_{0.5}PO_4:Tb^{3+}$, which exhibits a twofold increase in luminescence intensity compared to $YPO_4:Tb^{3+}$ [6].

The choice of yttrium orthophosphate as one of the components in the $Y_{1-x}Ln_xPO_4$ systems is because, along with gadolinium and lutetium compounds, it is most commonly used as a host matrix for mixed orthophosphates. In addition, it is isostructural with the orthophosphates of REEs, and the crystal ionic radius of yttrium (1.159 Å) differs only slightly from the radii of other REE ions (from 1.193 Å for Gd^{3+} to 1.117 Å for Lu^{3+}) [7]. Therefore, a continuous series of solid solutions between the components is possible in most of the previously described systems (see, *e.g.*, Refs. [1–3, 5, 6, 8–11]). In some works (*e.g.*, Refs. [4, 12, 13]), only individual fragments of continuous solid solution series were synthesized, as substitution limits were not reported.

At the same time, to the best of our knowledge, there is no literature data on $Y_{1-x}Ln_xPO_4$ systems (Ln = Gd–Lu, and Sc) with limited solid solution series. However, it is known [14–16] that, in general, continuous solid solution series should decompose upon cooling samples synthesized at high temperatures, forming limited composition ranges based on the system components.

The choice of YPO_4-based systems for the present study was also motivated by the absence of intrinsic luminescence in YPO_4 crystals down to 5 K [17].

Considering the above, before synthesizing solid solutions and studying the 'composition–property' relationships, it is desirable to know the limits of isomorphous substitutions and their thermodynamic stability under synthesis, intended use, and even storage conditions. Knowledge of the thermodynamic stability regions of solid solutions is essential for controlling their properties and ensuring their reproducibility over time and under varying temperatures.

Experimental determination of substitution limits and stability regions of solid solutions synthesized by the 'annealing and quenching' method using x-ray diffraction analysis (XRD) is complicated by the difficulty of achieving equilibrium at low temperatures due to the low diffusion rate in the solid phase, as well as by the possibility of partial decomposition upon cooling from high temperatures.

In addition, XRD may be of limited informativeness when the components are isostructural with very close sizes of the substituting structural units, as in the case of the $Y_{1-x}Dy_xPO_4$ system [4], in the case of spinodal decomposition of the solid solution [14–16], or when the studied samples are of nanoscale size, due to broadening and overlapping of x-ray reflections.

A lack of data on the limits of isomorphous substitutions and the stability regions of solid solutions forces researchers to select matrix and dopant compositions either by analogy with closely related systems or through a 'trial and error' approach. Such a method is often accompanied by excessive consumption of costly reagents and a significant increase in the time required for research. In this regard, it is advisable to use experimental methods and computational approaches that allow for a preliminary assessment of the stability of solid solutions and the substitution ranges, thus avoiding the mentioned limitations.

An example of such a rational approach can be found in studies [3, 5], where, in selecting the synthesis conditions for compounds in the $Y_{1-x}Sc_xPO_4$ system, the authors used calculation results for this system presented in Ref. [18].

It should be noted that nanoscale orthophosphates exhibit enhanced practically relevant properties due to their larger specific surface area. This is related to the fact that structural units located at the surface differ in coordination numbers from those inside the bulk, and this difference becomes more pronounced as the particle size decreases, leading to modifications of the material properties. As reported in Ref. [19], the conventional concepts of surface energy developed for macroparticles remain applicable to nanoparticles larger than 10 nm.

At the same time, it is known that in nanocrystalline materials with particle diameters above 6 nm, the volume of the surface layer remains smaller than that of the crystal interior [20]. Furthermore, according to Ref. [20], the structural characteristics of solid solutions do not depend on the particle size, at least within the range of 6-to-40–80 nm.

Based on the above considerations, the present work aimed to predict the thermodynamic stability and the limits of isomorphous substitutions in zircon-type orthophosphates of the composition $Y_{1-x}Ln_xPO_4$, where Ln = Gd–Lu, Sc. In this study, the calculated mixing energies (Q_{mix}), substitution limits (x), and critical decomposition temperatures (T_{cr}), obtained regarding the key energetic contributions (size-related, Q_R, and bond-ionicity contribution, Q_ε), provide a framework both for assessing the stability of $Y_{1-x}Ln_xPO_4$, including their nanoscale forms, and for selecting the optimal conditions for their synthesis.

2. INITIAL DATA AND CALCULATION METHOD

Within the Urusov's crystal-energy theory of isomorphous substitutions, the main challenge in determining the limits of isomorphous substitutions is finding the mixing energy. In the quasi-chemical approach, this corresponds to the interchange energy, and in the theory of subregular solid solutions, it corresponds to the interaction parameter [14–16]. Within the approximation of regular solid solutions, the critical (maximum) decomposition temperatures T_{cr} are calculated using Eq. (1) [14]:

$$T_{cr} = Q_{mix}/(2k_B N), \quad (1)$$

where Q_{mix} is the mixing energy, k_B is the Boltzmann's constant, and N is Avogadro's number.

In the considered systems, the relative differences in interatomic distances 'cation–tetrahedral anion' are significantly less than 0.1 (ranging from 0.0003 to 0.0411; Table 1). Therefore, according to Ref. [14], the calculation of solid-solution decomposition temperatures can be performed in the regular-solution approximation using

TABLE 1. Selected initial data, calculated mixing energies, and critical decomposition temperatures of solid solutions $Y_{1-x}Ln_xPO_4$, Ln = Gd–Lu, and Sc.

Ln	R, Å	$\Delta R/R_1 = (R_{Ln} - R_1)/R_1$	Q_R, kJ/mole	χ_{Ln}	$\chi(PO_4^{3-}) - \chi(Ln^{3+})$	ε_{Ln}	Δ_ε	Q_ε, kJ/mole	Q_{mix}, kJ/mole	T_{cr}, K
Gd	3.561	0.0177	4.250	1.386	2.314	0.712	0.010	0.618	4.868	291
Tb	3.537	0.0108	1.582	1.410	2.290	0.708	0.014	1.212	2.794	167
Dy	3.526	0.0077	0.804	1.426	2.274	0.705	0.017	1.787	2.591	155
Ho	3.512	0.0037	0.186	1.433	2.267	0.703	0.019	2.233	2.419	144
Er	3.498	0.0003	0.001	1.438	2.262	0.702	0.020	2.474	2.475	148
Tm	3.490	0.0026	0.092	1.455	2.245	0.695	0.027	4.521	4.613	275
Yb	3.480	0.0054	0.395	1.479	2.221	0.692	0.030	5.597	5.992	358
Lu	3.467	0.0092	1.148	1.431	2.269	0.704	0.018	2.023	3.171	189
Sc	3.361	0.0411	22.869	1.415	2.285	0.707	0.015	1.449	24.318	1452
Y	3.499	—	—	1.340	2.360	0.722	—	—	—	—

Becker's equation (Eq. (2)) [21]:

$$-\frac{1-2x}{\ln\dfrac{1}{1-x}} = \frac{R_g T_d}{Q_{mix}}, \qquad (2)$$

where x is the mole fraction of the dissolved component, R_g is the universal gas constant, and T_d is the solid-solution decomposition temperature. In both equations, R_g and Q_{mix} are expressed in calories [14].

Since the system components are isostructural, the mixing energy Q_{mix} was calculated using Urusov's equation (Eq. (3)), representing it as the sum of two contributions caused by differences in the degree of ionicity of the chemical bond in the system components (Q_ε) and the sizes of the substituting structural units (Q_R) [14–16]:

$$Q_{mix} = Q_\varepsilon + Q_R = \frac{1390 m z_m z_x \alpha(\Delta\varepsilon)^2}{2R} + C m n z_m z_x \left(\frac{\Delta R}{R_1}\right)^2 \text{ [kJ/mole]}, \qquad (3)$$

where $m = 2$—the number of different structural units in the system components in the pseudo-binary approximation of the zircon structure; $z_m = z_x = 3$—the charge magnitudes of the substituting and common structural units in the components; $\alpha = 1.723$—the reduced Madelung's constant calculated using Templeton's formula [22]; $C = 113$ kJ—an empirical value depending on compressibility and other crystal characteristics taken from Ref. [14]; $n = 6$—the coordination number of the substituting structural unit in the pseudo-binary approximation of the structure; R—interatomic distances 'cation–tetrahedral anion' Ln–PO_4 in the system components taken from Ref. [23]; ΔR and $\Delta R/R_1$—the difference and relative difference of interatomic distances 'cation–tetrahedral anion'; R_1—the interatomic distance in the system component with the smaller cation radius; $\Delta\varepsilon$—the difference in the degree of ionicity of the chemical bond in the system components.

The degrees of ionicity ε of the chemical bonds in the REE phosphate systems were determined based on the difference in electronegativities $\chi(Ln^{3+})$ of the cations [24] and the PO_4^{3-} anion. The electronegativity of the PO_4^{3-} anion was taken as 3.7 according to Batsanov [25].

3. RESULTS OF CALCULATIONS AND DISCUSSION

3.1. Mixing Energies of Solid Solutions

Some initial data and calculation results of the contributions Q_R,

caused by differences in the sizes of substituting structural units in the system components, to the total mixing energy Q_{mix}, are presented in Table 1 and Fig. 1, *a*.

As seen from the presented data, with increasing REE atomic number, the contributions Q_R, caused by differences in the sizes of substituting structural units, change smoothly. They decrease significantly from 4.250 to 0.001 kJ/mole along the series of solid solutions from $Y_{1-x}Gd_xPO_4$ to $Y_{1-x}Er_xPO_4$ and then increase to 1.148 kJ/mole in the series from $Y_{1-x}Er_xPO_4$ to $Y_{1-x}Lu_xPO_4$.

In the case of the $Y_{1-x}Sc_xPO_4$ system, the contribution Q_R is significantly larger (22.869 kJ/mole) because the crystal ionic radius of scandium is much smaller than those for the REEs [7], resulting in a larger size parameter $\Delta R/R_1$ for $Y_{1-x}Sc_xPO_4$, accordingly.

The smooth (regular) variation of Q_R values is apparently because the size parameter $\Delta R/R_1$ was calculated based on sufficiently accurate interatomic distances. The minimal values of Q_R in the middle of the dependence result from minimal differences in interatomic distances between the orthophosphate ions Y^{3+} (3.499 Å) and Ho^{3+} (3.512 Å), Er^{3+} (3.498 Å), and Tm^{3+} (3.490 Å).

The contributions caused by differences in the degree of ionicity of the chemical bond in the system components, Q_ε, to the total mixing energies Q_{mix} increase with the atomic number of the rare-earth element (REE) from Gd to Yb, rising from 0.618 to 5.597 kJ/mole, and then sharply decrease to 2.023 kJ/mole in the case of lutetium orthophosphate (Table 1, Fig. 1, *b*). This behaviour is due

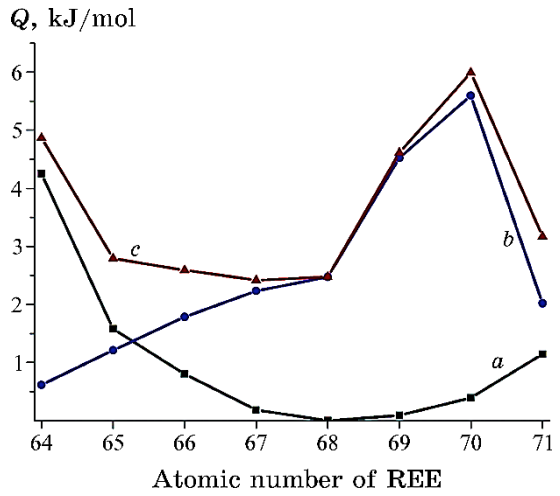

Fig. 1. Dependences of the contributions Q_R (curve *a*) and Q_ε (curve *b*) to the total mixing energies Q_{mix} (curve *c*) of solid solutions $Y_{1-x}Ln_xPO_4$, Ln = Gd–Lu, Sc, on the atomic numbers of the rare-earth elements.

to symbiotic changes both in the differences in ionicity degrees of the chemical bonds among the system components and in the electronegativities of the REEs.

The latter is explained by the fact that in the REE series, when moving from Tb to Yb, one electron is added to the 4*f*-sublevel of the REE with each step. In contrast, the transition from Yb to Lu does not add an electron to the 4*f*-sublevel but instead places it in the 5*d*-sublevel.

Overall, for REE orthophosphates from Dy to Lu, the total mixing energy Q_{mix} is mainly determined by contributions associated with differences in the degree of ionicity of the chemical bond Q_ε, while for Gd and Tb orthophosphates, the contributions due to differences in the sizes of substituting structural units Q_R dominate.

3.2. Substitution Limits and Thermodynamic Stability Regions

The decomposition temperatures T_d for limited solid-solution series were calculated using Eq. (2) for given substitution limits: $x = 0.01$, 0.03, 0.09, and 0.20 (Table 2). Based on the calculated decomposition temperatures (T_d) and critical decomposition temperatures (T_{cr}), their dependences on the atomic numbers of the REEs were plotted (Fig. 2).

These dependencies allow graphical determination, for limited solid solution series, of the equilibrium substitution limits x at given decomposition temperatures, or the decomposition temperatures at given substitution limits, for the orthophosphate systems ranging from Gd to Lu.

The intersection points of an isotherm drawn at the given decomposition temperature with a vertical line drawn from the REE atomic number enable estimating the composition interval within which the substitution limit lies. Interpolation along this vertical segment between the two closest curves then gives the substitution limit itself [26, 27]. The substitution limit can be refined by constructing, for a specific system, the dependence of the calculated decomposition temperatures (from Becker's equation) on the given composition, *i.e.*, by plotting the decomposition domes.

The calculated critical decomposition temperatures of the continuous solid solution series for the systems under consideration (Table 1, Fig. 2, *e*) are of 144–358 K for REEs orthophosphates and 1452 K for scandium orthophosphate. These values allow one to determine the temperature range for a continuous solid solution series. Thus, at $T > T_{cr}$ (curve *e*), the unlimited solid solutions are thermodynamically stable over the entire concentration range $0 \le x \le 1$. At $T < T_{cr}$, the unlimited solid solutions are unstable and may decompose into phases with limited solubility, if the diffusion rate and

TABLE 2. Decomposition temperatures (T_d [K]) of limited solid-solution series in the $Y_{1-x}Ln_xPO_4$ systems for substitution limits: $x = 0.01$, 0.03, 0.09, and 0.20.

Ln	Decomposition temperatures T_d [K] for substitution limit x			
	0.01	0.03	0.09	0.20
Gd	124	157	206	251
Tb	71	90	119	144
Dy	66	84	110	134
Ho	62	78	102	125
Er	53	80	105	128
Tm	117	149	195	238
Yb	153	193	254	310
Lu	81	102	134	164

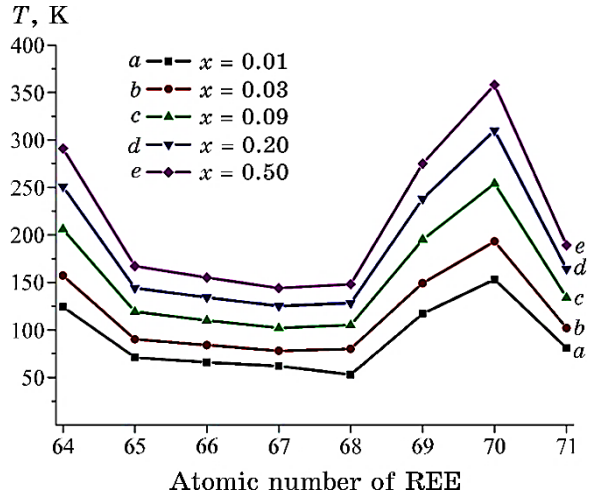

Fig. 2. Dependences of the calculated decomposition temperatures of solid solutions in the $Y_{1-x}Ln_xPO_4$ system on the REE numbers (thermodynamic stability diagram) for substitution limits $x = 0.01$ (*a*), $x = 0.03$ (*b*), $x = 0.09$ (*c*), $x = 0.20$ (*d*), and $x = 0.50$ (*e*).

time are sufficient for their formation.

It should be noted that the solid solutions in the $Y_{1-x}Ln_xPO_4$ systems have very low critical decomposition temperatures, with most of them even below room temperature. Consequently, they will remain stable over a wide temperature range from the critical temperatures up to the melting points of the system components, which exceed 2400 K [28]. This fact may indicate an advantage of materials based on continuous solid-solution series of yttrium orthophos-

phate with the composition $Y_{1-x}Ln_xPO_4$ in terms of property stability and reproducibility compared to similar materials based on solid solutions of other orthophosphates, such as scandium orthophosphate $Sc_{1-x}Ln_xPO_4$, whose critical temperatures range from 810 to 2880 K [18]. Moreover, materials based on continuous solid-solution series of the $Y_{1-x}Ln_xPO_4$ system may find preferential use in the production of nanomaterials by the sol–gel or low-temperature hydrothermal method, since nanomaterials are usually synthesized at low temperatures.

For all $Y_{1-x}Ln_xPO_4$ systems, where Ln = Gd–Lu, and Sc, the decomposition temperatures were calculated in the composition range $1.0 > x > 0$ with a step of $x = 0.05$, and decomposition domes were plotted (Figs. 3, 4). From these data, with greater accuracy than in Fig. 2, one can graphically determine the decomposition temperature for a given substitution limit, the substitution limit for a given temperature, and the regions of thermodynamic stability of the solid solutions. Above the peaks of the decomposition domes, continuous solid-solution series will be stable; below the peaks but above the dome lines, two limited solubility regions will exist; below

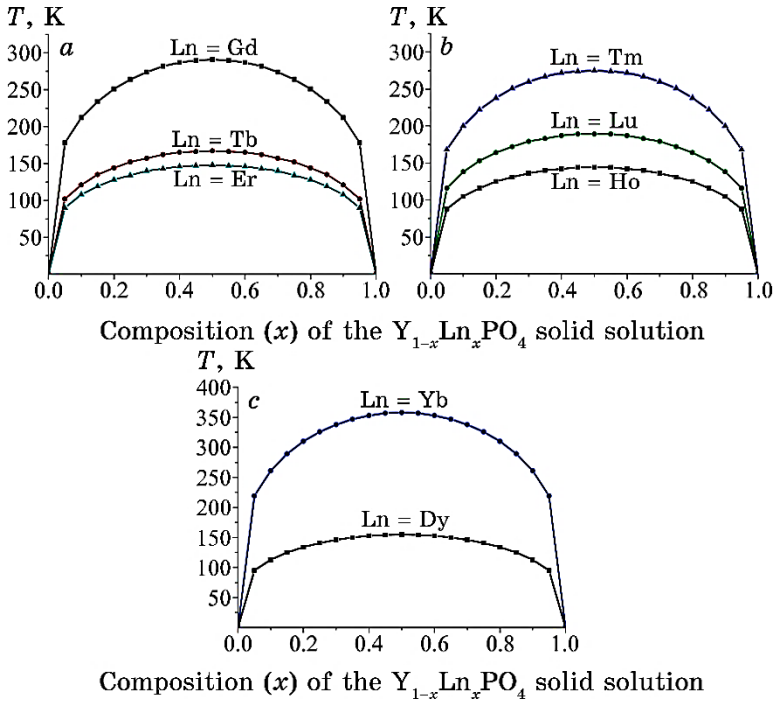

Fig. 3. Decomposition domes of solid solutions in the $Y_{1-x}Ln_xPO_4$ systems: (*a*) Ln = Gd, Tb, Er; (*b*) Ln = Ho, Tm, Lu; (*c*) Ln = Dy, Yb.

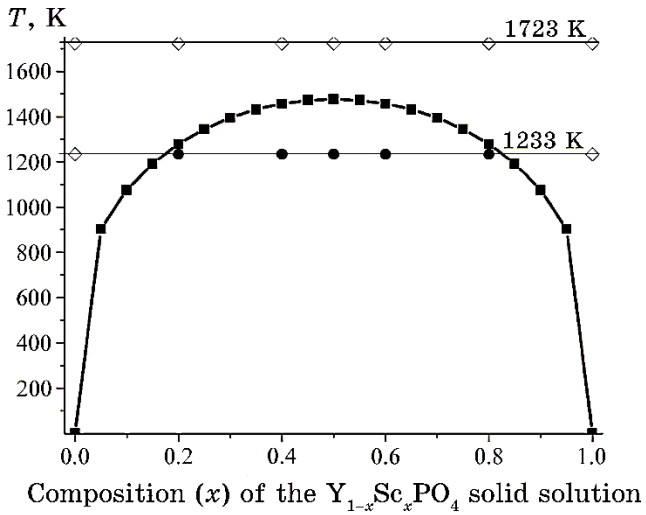

Fig. 4. Decomposition dome of the $Y_{1-x}Sc_xPO_4$ solid solution (■) and experimental data on synthesis temperatures for samples at 1233 K [3] and 1723 K [3, 5] (single-phase ◇ and multiphase ● samples).

the dome lines, mixtures of two solid solutions based on each component of the systems will be present.

4. COMPARISON OF CALCULATION RESULTS WITH LITERATURE DATA

Since the size parameters $\Delta R/R_1$ for the substitution of yttrium by scandium (Table 1), or scandium by yttrium [18], are less than 0.1 and equal, the solid solutions in the $Y_{1-x}Sc_xPO_4$ [3, 5] and $Sc_xY_{1-x}PO_4$ [11] systems can be considered within the regular solution approximation [14], and the calculated critical decomposition temperatures for both solid solutions will be practically identical.

To our knowledge, there is no literature on the critical decomposition temperatures, thermodynamic stability, or substitution limits for the $Y_{1-x}Ln_xPO_4$ solid solution systems with limited component solubility. Of course, this complicates the assessment of the reliability of the performed calculations.

However, there are reports on the synthesis temperatures of specific solid-solution compositions (Table 3). As seen from the data in Table 3, in most of the cited works (12 out of 13), the synthesis temperatures exceed the calculated critical decomposition temperatures, above which a continuous series of solid solutions exists in these systems. This indicates that the calculation results do not contradict the experimental literature data in the sense that synthe-

TABLE 3. Comparison of calculated T_{cr} results with synthesis temperatures from experimental studies*.

Composition, Ref.	x or %	Synthesis method	Synthesis temperature, K	T_{cr}, K
$Y_{1-x}Lu_xPO_4$ [2]	0.0, 0.25, 0.50, 0.75, 1.00	Precipitation from aqueous solutions	293–383; 773	189
$Y_{1-x}Sc_xPO_4$:0.5 mol.% Eu^{3+} [3]	0, 0.2, 0.4, 0.5, 0.6, 0.8, 1,0	Sol–gel method + annealing	1233 + 1723	1452
$Y_{1-x}Dy_xPO_4$ [4]	0.01, 0.05, 0.475	Sol–gel method with microwave–hydrothermal (MW–HT) treatment	473	155
$Y_{1-x}Sc_xPO_4$ [5]	0, 0.01, 0.05, 0.10, 0.2, 0.4, 0.5, 0.6, 0.8, 1.0	Solid-state method	1723	1452
$(Gd_xY_{1-x})_{1-y}PO_4$:yTb^{3+} (y = 0 or 0.15) [6]	0, 0.25, 0.5, 1.0	Solvothermal method	433 + 1023 + + 1273	291
$Y_{0.95(1-x)}Yb_{0.95x}Er_{0.05}PO_4$ [8]	0, 0.3, 0.5, 0.7, 1.0	MW–HT	473	358
$Y_{1-x}Yb_xPO_4$ [9]	$0 < x < 1$	Solid-state method	1473	358
YPO_4 doped with Tm^{3+} (0.1, 0.3, 0.5, 1 mol.%)/Yb^{3+} (10 mol.%) [10]	0.001, 0.003, 0.005, 0.01 (for Tm^{3+}); 0.10 (for Yb^{3+})	Co-precipitation from aqueous solution followed by annealing	333, 1073	275 (for Tm^{3+}); 358 (for Yb^{3+})
$Sc_xY_{1-x}PO_4$:0.5 мол.% Eu^{3+} [11]	0, 0.2, 0.4, 0.5, 0.6, 0.8, or 1.0	Sol–gel method + annealing	1373	1450
$Y_{1-x}Dy_xPO_4$ [12]	0.005–0.1	Flux growth technique	1673–1073	155
$Y_{1-x}PO_4$:xYb^{3+} [13]	0–0.1	Low-temperature hydrothermal method	473	358

Notes: *1. References [2, 6] provide synthesis and subsequent annealing temperatures of nanomaterials aimed at eliminating defects that, according to Refs. [29–31], are typically present in nanomaterials obtained at low temperatures. 2. References [3, 11] list only the annealing temperatures after synthesis by the sol–gel method. 3. References [4, 12, 13] do not specify substitution limits; it is possible that fragments of continuous series of solid solutions were synthesized.

sis was carried out within the thermodynamic-stability regions of solid solutions predicted by us.

At the same time, the synthesis of zircon-type solid-solution samples in the $Y_{1-x}Sc_xPO_4$:0.5 mol.% Eu^{3+} [3] and $Sc_xY_{1-x}PO_4$:0.5 mol.% Eu^{3+} [11] systems have been described, carried out by annealing mixtures of the components at 1233 and 1373 K, respectively. Under these conditions, according to XRD data, continuous solid-solution series were formed, as reported in those studies. However, in the luminescence spectra, which, according to the authors of Ref. [3], are more sensitive than XRD, additional bands were observed, indicating the multiphase nature of the synthesized samples. This agreed with our previously calculated [18] critical decomposition temperature for these solid solutions (1450 K), according to which, at 1233 and 1373 K, a continuous solid-solution series should not form (Fig. 4). Therefore, considering the critical decomposition temperature reported by us in Ref. [18], the authors of Refs. [3, 5] annealed $Y_{1-x}Sc_xPO_4$:0.5 mol.% Eu^{3+} samples at 1723 K, obtaining a continuous solid-solution series (Table 3, Fig. 4).

It should be noted that the orthophosphates $Y_{1-x}Lu_xPO_4 \cdot nH_2O$ ($x = 0.0$, 0.25, 0.50, 0.75, and 1.00) obtained in Ref. [2] at 293–383 K were nanosized (particle size of 5–10 nm); after calcination at 773 K, the particle size increased to 10–20 nm, and after calcination at 1373 K, it further increased to 40–80 nm.

The $Y_{1-x}Dy_xPO_4$ samples synthesized in Ref. [4] exhibited a high degree of crystallinity, with average particle sizes determined by transmission electron microscopy of 40 ± 15 nm for $x = 0.01$, 65 ± 22 nm for $x = 0.475$, and 125 ± 45 nm for $x = 1$.

The $GdPO_4$ powders obtained in Ref. [6] consisted of nanowires with lengths of 600 nm–3 μm and diameters of 20–70 nm; for $Gd_{0.75}Y_{0.25}PO_4$, the nanorods of 100–600 nm in length and 40–80 nm in diameter were observed, whereas, for $Gd_{0.5}Y_{0.5}PO_4$, the nanorods were of 100–400 nm in length and 50–100 nm in diameter. In contrast, YPO_4 powders displayed a rice-grain-like morphology, with particle sizes of 60–100 nm. Analysis of the data in Ref. [6] clearly shows that the amount of Y substituting for Gd in the $GdPO_4$ matrix affects the length-to-diameter ratio of the nanorods' morphology.

The particle sizes of $Y_{0.95(1-x)}Yb_{0.95x}Er_{0.05}PO_4$ ($x = 0$, 0.3, 0.5, 0.7, and 1) obtained in Ref. [8], as estimated from transmission electron microscopy images, ranged from 20 to 45 nm.

The average particle size of YPO_4 doped with Tm^{3+} (0.3 mol.%) and Yb^{3+} (10 mol.%) was approximately of 140 nm [10]. At the same time, the average crystallite sizes of YPO_4 doped with Tm^{3+} (0.1, 0.3, 0.5, and 1 mol.%) at a fixed Yb^{3+} concentration (10 mol.%) were 23, 22, 21, and 22 nm, respectively [10].

According to TEM data, $Y_{1-x}Yb_xPO_4$ particles ($x = 0$–0.1) exhibited a leaf-like nanomorphology with particle sizes of about 80 nm in

length and of about 16 nm in width [13].

Thus, comparison of the calculated critical decomposition temperatures with the synthesis data (Table 3) shows that the compositions obtained by sol–gel, hydrothermal, or microwave methods at 293–473 K [2, 4, 6, 8, 10, 13] are formed under conditions in which surface effects of nanoscale particles may significantly influence thermodynamic stability. At the same time, the calculated T_{cr} values for these systems are lower than the synthesis temperatures that confirms the applicability of the crystal-energy theory of isomorphous miscibility for predicting the conditions of nanoparticle formation. Therefore, the proposed computational approach optimizes the synthesis conditions, including those of nanocrystalline forms obtained at relatively low temperatures.

4. CONCLUSIONS

1. It has been shown that in the $Y_{1-x}Ln_xPO_4$ systems, the Q_ε contributions to the mixing energies Q_{mix} increase with the atomic number of the rare-earth element (REE) in the series of systems involving orthophosphates from Gd to Yb and, in most cases, determine the total values of the mixing energies (in 6 out of 8 systems, except for those involving Gd and Tb orthophosphates).
2. It has been established that the Q_R contributions to the mixing energy decrease in the Gd–Er series from 4.250 to 0.001 kJ/mole, and then increase to 1.148 kJ/mole in the Er–Lu series. Such variations in Q_ε and Q_R lead to nearly identical values for the total mixing energies and the critical decomposition temperatures of solid solutions in systems involving Tb, Dy, Ho, and Er orthophosphates.
3. A thermodynamic stability diagram for the $Y_{1-x}Ln_xPO_4$ (Ln = Gd–Lu) systems and decomposition domes for the $Y_{1-x}Ln_xPO_4$ (Ln = Gd–Lu, and Sc) systems are presented, enabling graphical prediction of solid-solution decomposition temperatures for given substitution limits, equilibrium substitution limits for a given temperature, and thermodynamic stability regions.
4. It has been established that most $Y_{1-x}Ln_xPO_4$ systems have critical decomposition temperatures either much lower than room temperature (systems $Y_{1-x}Tb_xPO_4$, $Y_{1-x}Dy_xPO_4$, $Y_{1-x}Ho_xPO_4$, $Y_{1-x}Er_xPO_4$, and $Y_{1-x}Lu_xPO_4$) or, within the calculation error, close to room temperature ($Y_{1-x}Gd_xPO_4$, $Y_{1-x}Tm_xPO_4$, and $Y_{1-x}Yb_xPO_4$). Therefore, they may be promising to produce nanomaterials, as the latter are synthesized at comparatively low temperatures.
5. Due to the extensive temperature range of thermodynamic stability (of about 2000 K), materials based on yttrium orthophosphate solid solutions $Y_{1-x}Ln_xPO_4$ may surpass materials based on solid

solutions of other REE orthophosphates in terms of stability of properties and reproducibility.

6. It has been shown that the calculation results do not contradict the experimental literature data in the sense that the synthesis of solid solutions in the $Y_{1-x}Ln_xPO_4$ systems in [2–6, 8–10, 12, 13] was carried out within the thermodynamic stability regions predicted by us. In addition, our calculated critical decomposition temperature for $Y_{1-x}Sc_xPO_4$, as well as the previously reported value for $Sc_{1-x}Y_xPO_4$ [18], agree with the results of Refs. [3, 5] concerning the choice of synthesis conditions for $Y_{1-x}Sc_xPO_4$.
7. Since the critical decomposition temperatures, substitution limits, and regions of thermodynamic stability of solid solutions are derived from the mixing energy Q_{mix}, which in the systems considered is governed primarily by differences in the interatomic distances of the components, and given that these distances have been shown in Ref. [20] to be independent of nanoparticle size in the range of 6-to-40–80 nm, the quantitative theory of isomorphous miscibility can be confidently applied for predicting isomorphous substitutions in particles larger than 6 nm.

ACKNOWLEDGMENTS

This research was carried out with the support of the Ministry of Education and Science of Ukraine within the framework of the priority areas of scientific development of the accredited research direction ‘Natural and Mathematical Sciences’ at Vasyl’ Stus Donetsk National University.

REFERENCES

1. V. S. Levushkina, D. A. Spassky, E. M. Aleksanyan, M. G. Brik, M. S. Tretyakova, B. I. Zadneprovski, and A. N. Belsky, *J. Lumin.*, **171**: 33 (2016); https://doi.org/10.1016/j.jlumin.2015.10.074
2. A. V. Osipov, L. P. Mezentseva, I. A. Drozdova, S. K. Kuchaeva, V. L. Ugolkov, and V. V. Gusarov, *Glass Phys. Chem.*, **33**, No. 2: 169 (2007); https://doi.org/10.1134/S1087659607020125
3. V. S. Voznyak-Levushkina, A. A. Arapova, D. A. Spassky, I. V. Nikiforov, and B. I. Zadneprovski, *Phys. Solid State*, **64**, No. 11: 567 (2022); https://doi.org/10.1134/S1063783422110130
4. Yu. V. Orlovskii, A. S. Vanetsev, I. D. Romanishkin, A. V. Ryabova, K. K. Pukhov, A. E. Baranchikov, E. V. Samsonova, K. Keevend, I. Sildos, and V. B. Loschenov, *Opt. Mater. Express*, **5**, No. 5: 1230 (2015); https://doi.org/10.1364/OME.5.001230
5. D. Spassky, A. Vasil’ev, V. Nagirnyi, I. Kudryavtseva, D. Deyneko, I. Nikiforov, I. Kondratyev, and B. Zadneprovski, *Materials*, **15**, No. 19: 6844 (2022); https://doi.org/10.3390/ma15196844

6. A. G. Hernández, D. Boyer, A. Potdevin, G. Chadeyron, A. G. Murillo, F. de J. C. Romo, and R. Mahiou, *Opt. Mater.*, **73**: 350 (2017); https://doi.org/10.1016/j.optmat.2017.08.034
7. R. D. Shannon, *Acta Crystallogr. Sect. A*, **A32**, No. 5: 751 (1976); https://doi.org/10.1107/S0567739476001551
8. S. A. Khrushchalina, P. A. Ryabochkina, V. M. Kyashkin, A. S. Vanetsev, O. M. Gaitko, and N. Yu. Tabachkova, *JETP Lett.*, **103**, No. 5: 302 (2016); https://doi.org/10.1134/S0021364016050064
9. O. Ya. Manashirov, A. N. Georgobiani, V. B. Gutan, E. M. Zvereva, and A. N. Lobanov, *Inorg. Mater.*, **47**, No. 12: 1384 (2011); https://doi.org/10.1134/S0020168511110124
10. H. Thakur, A. K. Gathania, S. Kachhap, S. K. Singh, and R. K. Singh, *J. Lumin.*, **254**, Pt. A: 119513 (2023); https://doi.org/10.1016/j.jlumin.2022.119513
11. D. Spassky, V. Voznyak-Levushkina, A. Arapova, B. Zadneprovski, K. Chernenko, and V. Nagirnyi, *Symmetry*, **12**, No. 6: 946 (2020); https://doi.org/10.3390/sym12060946
12. R. Faoro, F. Moglia, M. Tonelli, and E. Cavalli, *Physics Proc.*, **2**, No. 2: 345 (2009); https://doi.org/10.1016/j.phpro.2009.07.018
13. G. Wang, L. Gao, H. Zhu, and W. Zhou, *Front. Mater. Sci.*, **10**, No. 2: 197 (2016); https://doi.org/10.1007/s11706-016-0340-1
14. V. S. Urusov, *Teoriya Izomorfnoi Smesimosti* [The Theory of Isomorphous Miscibility] (Moskva: Nauka: 1977) (in Russian).
15. V. S. Urusov, *Fortschr. Mineral.*, **52**: 141 (1975).
16. V. S. Urusov, *Bulletin de la Société Française de Minéralogie et de Cristallographie*, **97**: 217 (1974); https://www.persee.fr/doc/bulmi_0037-9328_1974_act_97_2_6883
17. V. S. Levushkina, *Lyuminestsentnyye i Strukturnyye Svoistva Smeshannykh Kristallofosforov na Osnove Slozhnykh Oksidov* [Luminescent and Structural Properties of Mixed Crystal Phosphors Based on Complex Oxides] (Disser. for Degree Cand. Phys.-Math. Sci.) (Moskva: MSU: 2016) (in Russian); https://istina.ipmnet.ru/download/28937563/1uiTpO:H-EY-8zVYEzmDTCZfEKgNk8tBXdEO5Evd9jhyf8iFhs/
18. E. I. Get'man, S. V. Radio, and L. I. Ardanova, *Inorg. Mater.*, **54**, No. 6: 596 (2018); https://doi.org/10.1134/S0020168518060031
19. C. P. Poole Jr. and F. J. Owens, *Introduction to Nanotechnology* (John Wiley&Sons: 2003).
20. A. I. Grabchenko, L. I. Pupanj, L. L. Tovazhnyansky, *Vvedenie v Nanotekhnologii: Tekst Lektsiy* [Introduction to Nanotechnology: Lecture Notes] (Kharkiv: National Technical University «KhPI»: 2012) (in Russian).
21. R. Becker, *Z. Metallkunde*, **29**: 245 (1937) (in German).
22. D. H. Templeton, *J. Chem. Phys.*, **21**, No. 11: 2097 (1953); https://doi.org/10.1063/1.1698788
23. E. I. Get'man, *Izomorfnyye Zameshcheniya v Vol'framatnykh i Molibdatnykh Sistemakh* [Isomorphic Substitutions in Tungstate and Molybdate Systems] (Novosibirsk: Nauka: 1985) (in Russian).
24. K. Li and D. Xue, *J. Phys. Chem. A*, **110**, No. 39: 11332 (2006); https://doi.org/10.1021/jp062886k
25. S. S. Batsanov, *Strukturnaya Khimiya. Fakty i Zavisimosti* [Structural Chemistry. Facts and Dependences] (Moskva: Dialog-MGU: 2000) (in Russian).

26. E. I. Get'man and S. V. Radio, *Inorg. Mater.*, **53**, No. 7: 718 (2017). https://doi.org/10.1134/S0020168517070044
27. E. I. Get'man, S. V. Radio, L. B. Ignatova, and L. I. Ardanova, *Russ. J. Inorg. Chem.*, **64**, No. 1: 118 (2019); https://doi.org/10.1134/S0036023619010091
28. L. A. Boatner, *Rev. Mineral. Geochem.*, **48**, No. 1: 87 (2002); https://doi.org/10.2138/rmg.2002.48.4
29. R. Calderyn-Villajos, C. Zaldo, and C. Cascales, *Physics Proc.*, **8**: 109 (2010); https://doi.org/10.1016/j.phpro.2010.10.020
30. K. Lenczewska, M. Ptak, V. Boiko, K. Ledwa, and D. Hreniak, *J. Alloys Compd.*, **860**: 158393 (2021); https://doi.org/10.1016/j.jallcom.2020.158393
31. O. Savchuk, J. J. C. Marti, C. Cascales, P. Haro-Gonzalez, F. Sanz-Rodríguez, M. Aguilo, and F. Diaz, *Nanomaterials*, **10**, No. 5: 993 (2020); https://doi.org/10.3390/nano10050993